Recoil Proton Polarization in DVCS as a new probe for CFF $\mathcal{E}$

Olga Bessidskaia Bylund,* Maxime Defurne, and Pierre Guichon

IRFU, CEA Saclay

August 15, 2022

1 Introduction

While protons can be found all around us in the nuclei in all elements, yet many questions about their nature are yet unanswered. For instance, how does the proton acquire its mass? How is its spin decomposed? And how are the constituent quarks and gluons distributed inside the proton? Such questions can be addressed in the framework of Generalized Parton Distributions (GPDs), which correlate the transverse position with the longitudinal momentum of the partons inside a nucleon, thus allowing for the performance of nucleon tomography in terms of spatial distributions. GPDs are experimentally accessible through Compton Form Factors (CFFs) via measurements of exclusive processes, such as Deeply Virtual Compton Scattering (DVCS).

We are considering DVCS on a stationary proton target, using an electron beam. In the simplest case of leading order in perturbation theory and leading twist, the electron (momentum k) emits a virtual photon (q) that interacts with a single quark from the proton (p). The quark then emits a real photon (q') before being reabsorbed by the proton (p'), as illustrated in Fig. 1. The DVCS process is governed by the following parameters: the beam energy E_k, the virtuality of the exchanged photon Q^2, $x_B = Q^2/(2pq)$, the momentum transfer to the proton $t = (p' - p)^2$ and the angle ϕ_h between the hadronic plane, spanned by the directions of the scattered proton and the produced photon, with respect to the leptonic plane, spanned by the initial and the scattered lepton directions.

From the factorization theorem, the process can be split into a hard part, where perturbation theory is applicable, and a soft part that can be parameterized by GPDs, encoding the structure of the nucleon. At leading order and leading twist, four GPDs ($H, E, \tilde{H}, \tilde{E}$) can describe DVCS, each having the corresponding CFF ($\mathcal{H}, \mathcal{E}, \tilde{\mathcal{H}}, \tilde{\mathcal{E}}$). For this work the unconstrained $\tilde{\mathcal{E}}$ has been set to zero throughout.

Conventionally, in fixed target experiments, $\mathcal{H}$ is measured using an unpolarized target, $\tilde{\mathcal{H}}$ with a longitudinally polarized target and $\mathcal{E}$ with a transversely polarized target, see e.g. [1]. Maintaining a transversely polarized target is experimentally challenging and restricts the setup to a low beam current and hence a low luminosity. Another method is to measure $\mathcal{E}$ with a neutron target, as done by the Hall A collaboration at Jefferson Lab [2], exploiting that DVCS on the neutron has higher sensitivity to $\mathcal{E}$ than on the proton. From a theoretical point of view though, this introduces the complications of interactions between

---

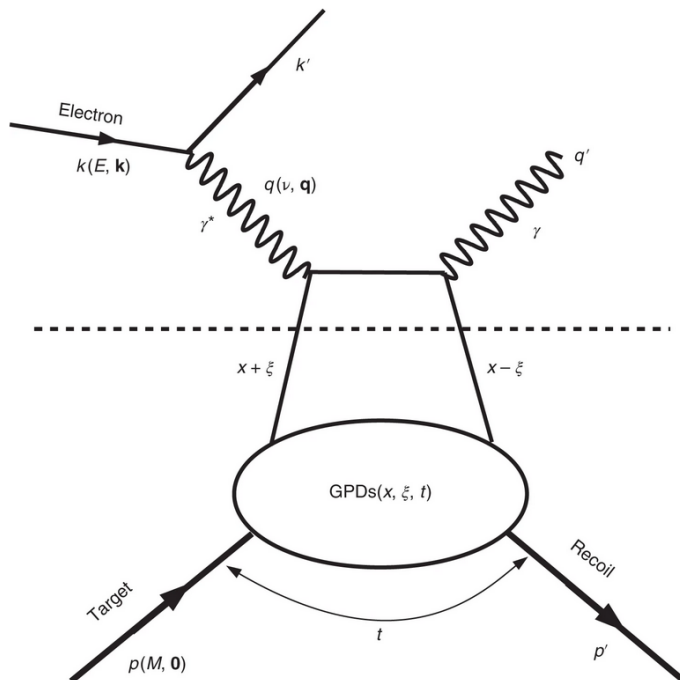*Electronic address: olgabylund@gmail.com; Corresponding author

Figure 1: A schematic diagram of the DVCS process. An electron with momentum k interacts via a virtual photon of momentum q with a stationary proton. The electron is scattered with momentum k', a real photon with momentum q' is produced, and the stationary proton (p) gets scattered with momentum p' The dashed line illustartes the factorization of the process into an (upper) perturbative part and a (lower) non-perturbative one.

the spectator proton and the neutron as well as possible modifications of the neutron structure when compared to free neutrons. In our study, we propose the polarization of the recoil proton as an alternative observable and investigate its sensitivity to CFF $\mathcal{E}$.

2   The polarization of the recoil proton

CFF $\mathcal{E}$ describes exclusive reactions where the nucleon changes helicity during the interaction. This leads us to propose the polarization of the recoil proton in DVCS as alternative observable for $\mathcal{E}$. Such a measurement could be performed using an unpolarized target, thus allowing for much higher luminosities. The polarization along the direction normal to the hadronic plane P_y is found to be sensitive to CFF $\mathcal{E}$, particularly at $\phi_h = \pi$, where all scattered particles can be found in the same plane. The dependence of P_y on ϕ_h is shown in Figure 2.

The transverse polarization of a proton can be measured by rescattering it on a secondary target, such as carbon. An azimuthal dependence is then induced with the coefficient proportional to the transverse polarization. A set of trackers before and after the analyzer allow the determination of the scattering angles in the polarimeter θ_{pol} and ϕ_{pol}. We are currently using a convention for ϕ_{pol} where this dependence is parameterized as:

$$\frac{\mathrm{d}N}{\mathrm{d}\theta_{pol}} = N_0(1 + \frac{\mathrm{d}\epsilon}{\mathrm{d}\theta_{pol}} A_p(P_y \sin \phi_{pol} - P_x \cos \phi_{pol})). \qquad (1)$$

Here θ_{pol} is the rescattering polar angle, $\frac{\mathrm{d}\epsilon}{\mathrm{d}\theta_{pol}}$ the differential efficiency, A_p the analyzing power and ϕ_{pol} the azimuthal rescattering angle.

The analyzing power of the polarimeter gives the sensitivity to the transverse polarization, while the efficiency gives the probability for the proton to undergo a useful scattering in the analyzer. Both quantities have a dependence on the proton momentum and the rescattering polar angle in the polarimeter θ_{pol}. The
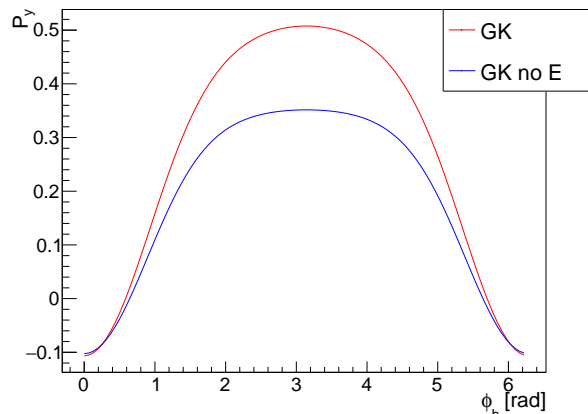
Figure 2: P_y as a function of the variable ϕ_h for the configuration $E_k = 10.6\,\text{GeV}$, $Q^2 = 1.8\,\text{GeV}^2$, $x_B = 0.17$, $t = -0.45\,\text{GeV}^2$ and an unpolarized lepton beam.

efficiency also has a dependence on the thickness of the analyzer, which is set to 15cm in this work. The efficiency is calculated according to the expression given in [3] and the analyzing power using McNaughton's parametrization [4]. It is found that the analyzing power is highest when the kinetic energy of the proton is around 200 MeV, see Fig. 3. With the efficiency integrated over the range of 4-19° in θ_{pol} being below 0.1, this requires a high luminosity.
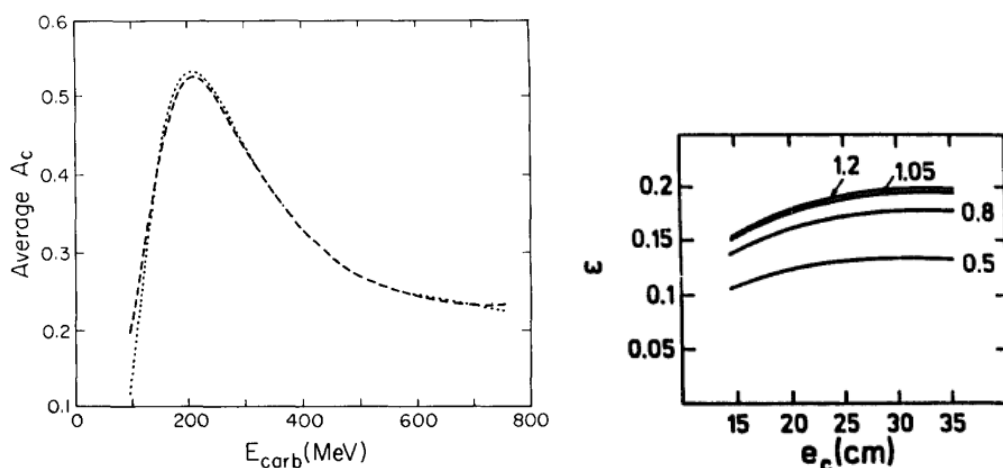

Figure 3: The analyzing power as a function of the proton kinetic energy at the centre of the carbon analyzer [4] (left) and the efficiency for different kinetic energies in GeV [3] (right).

The overall performance of such a polarimeter is given by a convolution of the efficiency with the analyzing power in quadrature:

$$F^2 = \int_{\theta_{min}}^{\theta_{max}} A_p(\theta)^2 \epsilon(\theta) \mathrm{d}\theta \,. \qquad (2)$$

Hence in a tradeoff between high efficiency at higher energies and high analyzing power at lower energies, the analyzing power has higher impact on the performance of the polarimeter.

3   Optimization

The study is done in the context of Hall C at Jefferson Lab, assuming a beam current of $10\mu A$, which is much higher than is typically used in experiments with a transversally polarized target, and 18 days of data taking. We are currently

considering an unpolarized electron beam. At Hall C, the scattered electron can be detected by the High Momentum Spectrometer (HMS) [5], while for photon detection a new Neutral Particle Spectrometer (NPS) [6] is being prepared.

In order to find a kinematic configuration that is optimal for constraining $\mathcal{E}$ in a polarization measurement, a figure of merit F' is constructed. It is inspired by the relation giving the precision to which the polarization can be determined δ_P, which depends on the polarimeter figure of merit F and the available statistics N: $\delta_P \propto \frac{1}{F\sqrt{N}}$. We replace the precision δ_P by the difference in polarization along the y-axis between the nominal hypothesis and the null hypothesis ΔP_y , i.e. when CFF $\mathcal{E}$ is set to zero. Thus, our figure of merit is

$$F' = F \cdot \Delta P_y \cdot \sqrt{N} \,, \tag{3}$$

with F being the figure of merit for the polarimeter. For our optimization we are considering the GK model [7], which displays high sensitivity of P_y to CFF $\mathcal{E}$.

The condition $|t|/Q^2 \leq 0.25$ is imposed to ensure factorization and the validity of the leading twist approximation. After a preoptimization with respect to F', the Geant4 simulation for Hall C is performed [8], including the simulation of the acceptance and efficiency of the HMS and the NPS when they are positioned to target the electron and photon with the momenta and scattering angles given in Table 1. Next, the DVCS parameters are varied around their preselected values in search for other configurations that give us better sensitivity post-simulation, thus taking detector acceptance into account.

In the end, the configuration $E_k = 10.6$ GeV, $Q^2 = 1.8$ GeV^2, $x_B = 0.17$, $t = -0.45$ GeV^2, $\phi_h = \pi$ is selected. The momenta and directions of the particles are determined solely by these parameters; they are given in Table 1. The electron and the photon scatter at small angles on either side of the beam, while the proton scatters at a large angle, on the same side of the beam as the scattered electron. The kinetic energy of a proton, with an initial momentum of 0.71 GeV/c, is 190 MeV at the center of a carbon analyzer of length 15 cm. Hence we have arrived at a configuration with a high analyzing power.

electron $|\mathbf{k}'|$	$\theta_{k'}$	photon $|\mathbf{q}'|$	$\theta_{q'}$	proton $|\mathbf{p}'|$	$\theta_{p'}$
4.96 GeV$/c$	10.6°	5.40 GeV$/c$	-15.1°	0.71 GeV$/c$	44°

Table 1: The momenta and angles of the scattered particles for our optimal configuration.

The predictions for the baseline and the null hypotheses for this configuration are given in Table 2 along with two other models, VGG [9] and KM15 [10], for comparison. We aim to discriminate the baseline hypothesis from the null hypothesis and from the predictions by the two other models.

Prediction	$\mathcal{H}$	$\mathcal{E}$	$\tilde{\mathcal{H}}$	P_y
GK	-1.1+5.4i	-2.4-0.4i	0.7+1.8i	0.50
GK no E	-1.1+5.4i	0	0.7+1.8i	0.36
VGG	-2.2+4.8i	-1.0+1.5i	0.5+1.4i	0.24
KM15	-2.9+3.2i	1.6+0i	0.5+1.5i	0.15

Table 2: The Compton Form Factors and the resulting polarization of the proton along the y-axis for the configuration $E_k = 10.6$ GeV, $Q^2 = 1.8$ GeV^2, $x_B = 0.17$, $t = -0.45$ GeV^2, $\phi = \pi$. $\tilde{\mathcal{E}}$ has been set to zero.

4   Toy fit

In the DVCS process, the proton can be scattered in any direction a priori. The directions of the detected electron and the photon are restricted by the acceptance

of the HMS and the NPS. In order to constrain the direction of the proton and to consider a more realistic setup, a toy simulation of a proton polarimeter with an acceptance of $40 \times 60°$ in $\theta_{p'} \times \phi_{p'}$ is performed. The polarimeter is centered on the targeted proton scattering angle $\theta_{p'}$ in the same plane as all the other particles (to target $\phi_h = \pi$). A polarimeter with this angular acceptance at a distance of 1 metre from the center of the target would cover approximately 1 str. With this selection, we expect 4.8 million events in total, of which only 3% will undergo a useful scattering in the analyzer. The scattered protons are assigned values of θ_{pol} following the expression for the differential efficiency and ϕ_{pol} following Eq. 1. Using an unpolarized beam, P_x will be 0 on average, so the expected distribution in ϕ_{pol} should be a sine function on top of a constant term, as seen in Fig. 4.
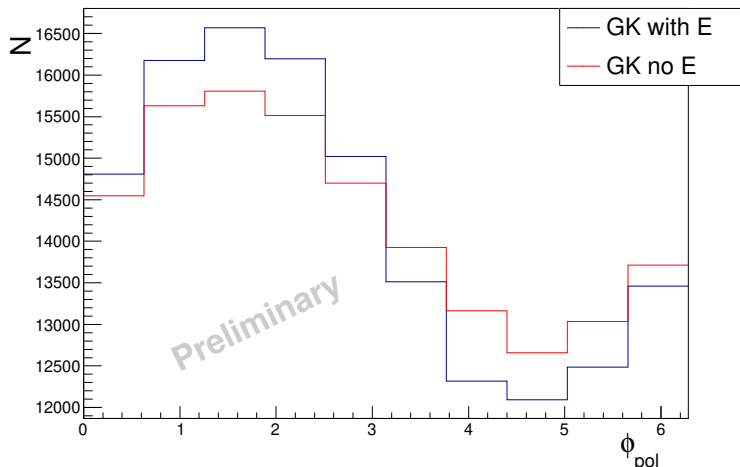

Figure 4: The distribution in $\phi_{pol.}$ after the toy simulation for the proton polarimeter.

Fitting this distribution for the two hypothesis for P_y gives $P_y(GK) = 0.475 \pm 0.011$ for the baseline hypotehsis and $P_y(\mathcal{E} = 0) = 0.316 \pm 0.011$ for the null hypothesis, consistent with the average value of the polarization distributions at 0.463 and 0.304 respectively.

5   Conclusions

We have here proposed the polarization of the recoil proton in DVCS events as an observable to constrain CFF $\mathcal{E}$. With a statistical analysis aimed at Hall C we have shown that enough statistics would be available to distinguish between the hypothesis with $\mathcal{E}$ and without $\mathcal{E}$ and also to tell apart the GK model prediction from the VGG and KM15 predictions. We have also identified a configuration that can be used as a starting point for a proposal.

References

[1] Kresimir Kumerički, Dieter Müller, and Morgan Murray. HERMES impact for the access of Compton form factors. *Phys. Part. Nucl.*, 45(4):723–755, 2014.

[2] Marija Čuić, Krešimir Kumerički, and Andreas Schäfer. Separation of Quark Flavors Using Deeply Virtual Compton Scattering Data. *Phys. Rev. Lett.*, 125(23):232005, 2020.

[3] B. Bonin, A. Boudard, H. Fanet, R.W. Fergerson, M. Garçon, C. Giorgetti, J. Habault, J. Le Meur, R.M. Lombard, J.C. Lugol, B. Mayer, J.P. Mouly, E. Tomasi-Gustafsson, J.C. Duchazeaubeneix, J. Yonnet, M. Morlet, J. Van de Wiele, A. Willis, G. Greeniaus, G. Gaillard, P. Markowitz, C.F. Perdrisat,

R. Abegg, and D.A. Hutcheon. Measurement of the inclusive p-c analyzing power and cross section in the 1 gev region and calibration of the new polarimeter pomme. *Nuclear Instruments and Methods in Physics Research Section A: Accelerators, Spectrometers, Detectors and Associated Equipment*, 288(2):379–388, 1990.

[4] M. W. Mcnaughton et al. THE P C ANALYZING POWER BETWEEN 100-MEV AND 750-MEV. *Nucl. Instrum. Meth. A*, 241:435–440, 1985.

[5] H. Mkrtchyan et al. The lead-glass electromagnetic calorimeters for the magnetic spectrometers in Hall C at Jefferson Lab. *Nucl. Instrum. Meth. A*, 719:85–100, 2013.

[6] Exclusive Deeply Virtual Compton and Neutral Pion Cross-Section Measurements in Hall C. PR12-13-010, `https://wiki.jlab.org/cuawiki/images/f/fa/User_Guide.pdf`, 2013.

[7] S. V. Goloskokov and P. Kroll. Vector meson electroproduction at small Bjorken-x and generalized parton distributions. *Eur. Phys. J. C*, 42:281–301, 2005.

[8] Ho San Ko. *Neutral Pion Electroproduction and development of a Neutral Particle Spectrometer*. Theses, Université Paris-Saclay ; Seoul National University, July 2020.

[9] M. Vanderhaeghen, Pierre A. M. Guichon, and M. Guidal. Deeply virtual electroproduction of photons and mesons on the nucleon: Leading order amplitudes and power corrections. *Phys. Rev. D*, 60:094017, 1999.

[10] Kumericki1a K. and M uller D. Description and interpretation of DVCS measurements, 2016.